Scripta Materialia 116 (2016) 82–86

Contents lists available at ScienceDirect

Scripta Materialia

journal homepage: www.elsevier.com/locate/scriptamat

Regular Article

Effects of natural aging after pre-aging on clustering and bake-hardening behavior in an Al–Mg–Si alloy

Yasuhiro Aruga [a,*], Masaya Kozuka [a], Yasuo Takaki [b], Tatsuo Sato [c,d]

[a] Materials Research Laboratory, Kobe Steel, Ltd., 1-5-5 Takatsukadai, Nishi-ku, Kobe 651-2271, Japan
[b] Aluminum Sheets and Coils Research Department, Aluminum & Copper Business, Kobe Steel, Ltd., 15 Kinugaoka, Moka, Tochigi 321-4367, Japan
[c] Tokyo Institute of Technology, Nagatsuta 4259-R2-18, Midori-ku, Yokohama 226-8503, Japan
[d] Aluminum & Copper Business, Kobe Steel, Ltd., 5-9-12 Kita-Shinagawa, Shinagawa-ku, Tokyo 141-8688, Japan

ARTICLE INFO

Article history:
Received 3 November 2015
Received in revised form 6 January 2016
Accepted 12 January 2016
Available online 7 February 2016

Keywords:
Aluminum alloys
Aging
Hardness
Atom probe tomography
Cluster

ABSTRACT

Atom probe tomography (APT) analysis was used to characterize the clustered state after pre-aging at 90 °C (PA) and subsequent natural aging (NA) in an Al–0.62Mg–0.93Si (mass%) alloy. It was revealed that larger Si-rich clusters increase in number after prolonged NA. The long-term NA after PA is believed to promote the preferential aggregation of solute Si toward clusters formed during PA rather than the independent formation of Si-based clusters. The prolonged NA inhibits the hardness increase during bake-hardening (BH) treatment at 170 °C. The deterioration of the BH response appears to be due to the increase of the Si-rich clusters.

Al–Mg–Si alloys are widely used as automobile body panels because of their desirable combination of good formability and high strengthening potential. The so-called paint-bake cycling process, a thermal cycling process [1] designed to provide both paint curing and precipitation-hardening for auto panels, involves a relatively short-duration artificial aging process. A typical paint-bake cycle of 30 min at 175 °C is much too short to reach peak strength, which requires 10–20 h at 175 °C for naturally pre-aged Al–Mg–Si alloys [2]. A typical precipitation sequence is as follows.

$$\alpha(\mathrm{SSSS}) \rightarrow \text{solute clusters} \rightarrow \text{GP zones} \rightarrow \beta'' \rightarrow \beta' \rightarrow \beta \quad (1)$$

where SSSS is the supersaturated solid solution [3]. Since the SSSS is very far from equilibrium, even natural aging (NA) at room temperature (RT) causes cluster formation. This is evidenced by a significant increase in hardness observed during NA [4].

Clusters strongly influence the precipitation of the β″ phase, widely recognized as the strengthening phase formed during artificial aging [5]. Hence, atom probe tomography (APT) has been used actively to characterize the clusters formed during aging after solution treatment [6–15]. It has been described that clusters formed during NA do not act as precursors of the β″ phase during subsequent artificial aging. This causes the so-called negative effect of NA, which results in a reduced strength after the paint-bake treatment. Si-rich clusters formed during NA can neither be dissolved nor grow further, resulting in the retardation of the hardness increase during artificial aging at 170 °C for up to 3.6 ks [14].

It is known that a pre-aging (PA) heat treatment in the temperature interval 70 °C to 120 °C after quenching leads to a higher number density of the β″ precipitates during subsequent artificial aging, resulting in an improved bake-hardening (BH) response [13,16,17]. It was believed that clusters with a uniform Mg/Si ratio, which are formed during PA can either transform to β″ or serve as nuclei for precipitation of β″ [13,18]. The clusters formed during PA prevent cluster formation and growth during subsequent NA, but the hardness increases after a long-time NA even if the PA is applied [19,20]. Regarding the clustering behavior during NA after PA, Takaki et al. [20] reported based on the calorimetry analyses that NA for a prolonged period of time after PA causes a change in clustered state and deteriorates the BH response. Although the alloy sheets for the automotive application are usually stored for a period at RT even though PA is conducted in industrial practice, there are very few reports about the clustering behavior during NA after PA. In the present study, the focus is made on the characterization of the clustered state after PA and subsequent prolonged NA. The detailed microstructural characterization using APT gives insight into the mechanism in the negative effect of NA after PA on the BH response in Al–Mg–Si alloys.

An ingot of Al–0.62Mg–0.93Si (mass%) alloy was manufactured using an air furnace, homogenized, hot rolled, and cold rolled down to

* Corresponding author.
E-mail address: aruga.yasuhiro@kobelco.com (Y. Aruga).

http://dx.doi.org/10.1016/j.scriptamat.2016.01.019

1.0 mm thickness. The material was fully recrystallized and solution treated in a salt bath at 570 °C for 1.8 ks followed by quenching into a hot water bath at 90 °C. Then NA was conducted at RT for 4.0×10^4 ks after PA at 90 °C for 18 ks. The hardness change during NA after PA was measured at RT using an Akashi AVK-C2 model Vickers hardness tester with a 49 N load and a dwell time of 15 s. Both the PA and PA + NA samples were subsequently aged in an oil bath at 170 °C for 3.6 ks to evaluate the BH response. The details of the heat treatment processes used in this work are summarized in Table 1.

Specimens for APT were cut from the sheets and electropolished using the standard two-stage method [21]. APT analyses were carried out using a LEAP™ 3000 HR instrument (CAMECA Instruments Inc.). The analyses were performed at a specimen temperature of 30 K, a voltage pulse fraction (pulse voltage/steady-state voltage) of 20% in a voltage range of 3.9–6.1 kV, and a pressure in the specimen chamber below 10^{-8} Pa. Visualization and quantitative evaluation of the 3-D atom-by-atom datasets were performed using the IVAS software 3.6.6 (CAMECA Instruments Inc.). Two separate experimental runs were carried out for each condition, and consistent results were obtained between the runs.

The maximum separation method [22] was used to select discrete regions enriched in solute atoms. This was done by grouping together solute Mg and Si atoms within a given distance d_{max} of one another ($d_{max} = 0.75$ nm in the present study). Then, the map of solute-rich regions was obtained by removing all groups that contained less than $N_{min} = 10$ solute atoms. N_{min} and d_{max} values were chosen so that no solute clusters were observed in a random solid solution of the same composition.

Change of the Vickers hardness during NA up to 7.8×10^4 ks after PA at 90 °C for 18 ks is shown in Fig. 1. There is no obvious difference in hardness during NA for up to approximately 1.5×10^3 ks. It can be seen that increasing the aging time beyond 1.5×10^3 ks causes a gradual increase in hardness, and that the hardness increases almost linearly with the logarithm of NA time.

Fig. 2 shows Vickers hardness before and after BH treatment at 170 °C for 3.6 ks in both materials after PA at 90 °C for 18 ks (PA), and after PA at 90 °C for 18 ks followed by NA for 4.0×10^4 ks (PA + NA). Hardness in the PA + NA material is higher than in the PA material before the BH treatment due to a long-term natural age-hardening. Hardness after the BH treatment is almost the same in both the materials, indicating that the prolonged NA after PA inhibits the hardness increase during the BH treatment (i.e., the BH response).

The APT analysis volumes and the quantitative information about the detected clusters are listed in Table 2. More than 8 million atoms were provided for the cluster analysis, and about 1000 clusters were obtained for each material. The radius of gyration and the associated Guinier radius [21] were used to define the sizes of the clusters. The average radius of the clusters was calculated from the total sum of the average values of the respective clusters divided by the whole cluster population. The results clearly show that NA after PA leads to an increase in the number density, whereas a decrease in the average Mg/Si ratio of clusters. The average radius of clusters in the PA + NA material is slightly larger than in the material without NA.

The size distribution of the clusters is shown in Fig. 3(a). A peak in the number density can be observed at approximately 1.2 nm in Guinier radius for both the PA and PA + NA materials. The number density of clusters in the PA + NA material is higher overall compared to the PA material. In other words, the number density of clusters increases, with no dependence on the cluster size during prolonged NA after PA. The relationship between the Mg/Si ratio and number density of the clusters is shown in Fig. 3(b). The plot labeled 1.0 in the Mg/Si ratio, in which the Mg/Si ratio is ranging from 0.8 to 1.0, has the highest number density in both the PA and PA + NA materials. The clusters have a wide range of Mg/Si ratio from close to 0 to over 2.0. It is evident that the number density of the clusters with low Mg/Si ratio (Mg/Si < 1.0) in the PA + NA material is remarkably higher than in the PA material. This indicates that Si-rich clusters mainly increase during the long-time storage at RT. Some works suggested that the Si-rich clusters are preferentially formed quickly after solution treatment, and Mg atoms diffuse to the clusters, eventually forming Mg–Si clusters after prolonged NA [13,16,23,24]. When just NA treatment is conducted for the same alloy as this work [13], the number fractions of the Si-rich cluster (Mg/Si ratio < 1.0) after a short storage (108 ks) and a long storage (2.8×10^4 ks) are 60% and 51%, respectively. The current study has revealed that the number fractions of the Si-rich clusters in the PA and PA + NA materials are 54% and 61%, respectively. It is certainly interesting that the proportion of the Si-rich clusters increases over such a long period of time at RT after PA, unlike the behavior in the materials without PA.

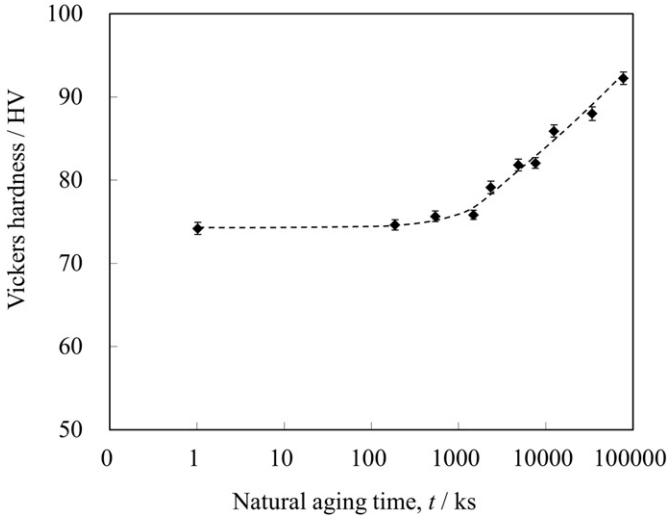

Fig. 1. Change of the Vickers hardness during NA after at 90 °C for 18 ks. Stated errors represent one standard error on the basis of five measurements per sample.

Table 1
Heat treatment processes after solution treatment; the terms NA, PA, BH represent natural aging at RT, pre-aging, and bake-hardening treatment at 170 °C for 3.6 ks, respectively.

Material number	Heat treatment process
PA	PA at 90 °C for 18 ks
PA + NA	PA at 90 °C for 18 ks and NA for 4.0×10^4 ks
PA + BH	PA at 90 °C for 18 ks and BH
PA + NA + BH	PA at 90 °C for 18 ks, NA for 4.0×10^4 ks and BH

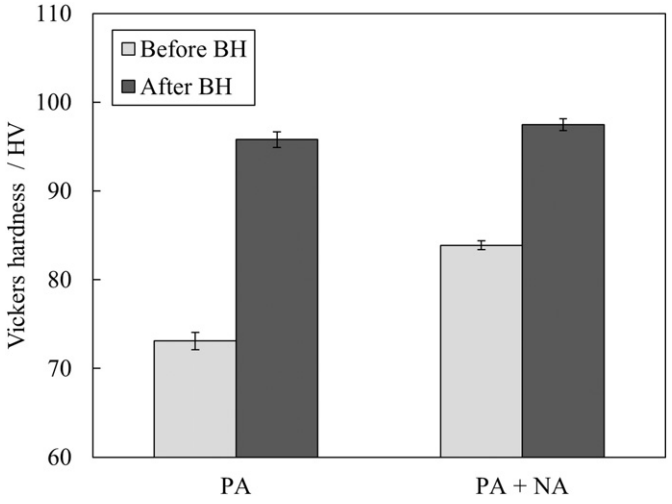

Fig. 2. Vickers hardness before and after BH treatment at 170 °C for 3.6 ks in the materials after PA at 90 °C for 18 ks (PA) and subsequent NA for 4.0×10^4 ks (PA + NA). Stated errors represent one standard error on the basis of five measurements per sample.

Table 2
Characteristic values describing the APT datasets and the overall population of clusters defined by the maximum separation method with $d_{max} = 0.75$ nm, $N_{min} = 10$.

	PA	PA + NA
Aging condition	90 °C, 18 ks	90 °C, 18 ks + RT, 4.0×10^4 ks
Number of atoms analyzed[a]	11 M	8.1 M
Number of clusters detected[a]	1075	1000
Number density of clusters (10^{24}/m^3)[b]	2.4 ± 023	3.0 ± 001
Average radius of clusters, r (nm)[b]	1.31 ± 002	1.35 ± 001
Average Mg/Si ratio of clusters[b]	1.07 ± 003	0.90 ± 003

[a] Total number of atoms or clusters in two measurements.
[b] Stated errors represent one standard error on the basis of two measurements per sample.

Fig. 4(a) represents the Mg/Si ratio of clusters plotted against cluster size ranges. Hardly any difference in the Mg/Si ratio is seen in the clusters with below 1.5 nm in radius, whereas the ratio of clusters with larger radius is considerably lower after NA than when no NA is given after PA. This indicates that the larger clusters, which are formed during prolonged NA after PA, have higher concentration of Si. Fig. 4(b) is average concentration profiles of Mg and Si with distance from the center of the larger clusters. The number of target clusters with radius larger than 1.5 nm is about 250 for each material. The radial distributions of Mg and Si were drawn from the average values of the respective clusters. Plots of radius less than 0.2 nm were filtered out of the profile, as they induce aberrant composition values. The centers of the clusters delineated by the leftmost data point for the figures are enriched in Mg and Si, which decrease toward the outside of clusters. It is revealed that no outstanding difference in the Mg concentration profiles between the PA and PA + NA materials, while the Si concentration in the PA + NA material is remarkably higher than in the PA material except for the region near the center of clusters as indicated by a circle and arrow in the figure. It is believed that a long-term NA after PA promotes the preferential aggregation of solute Si toward clusters formed during PA rather than the independent formation of Si-based clusters, and eventually forms larger Si-rich clusters.

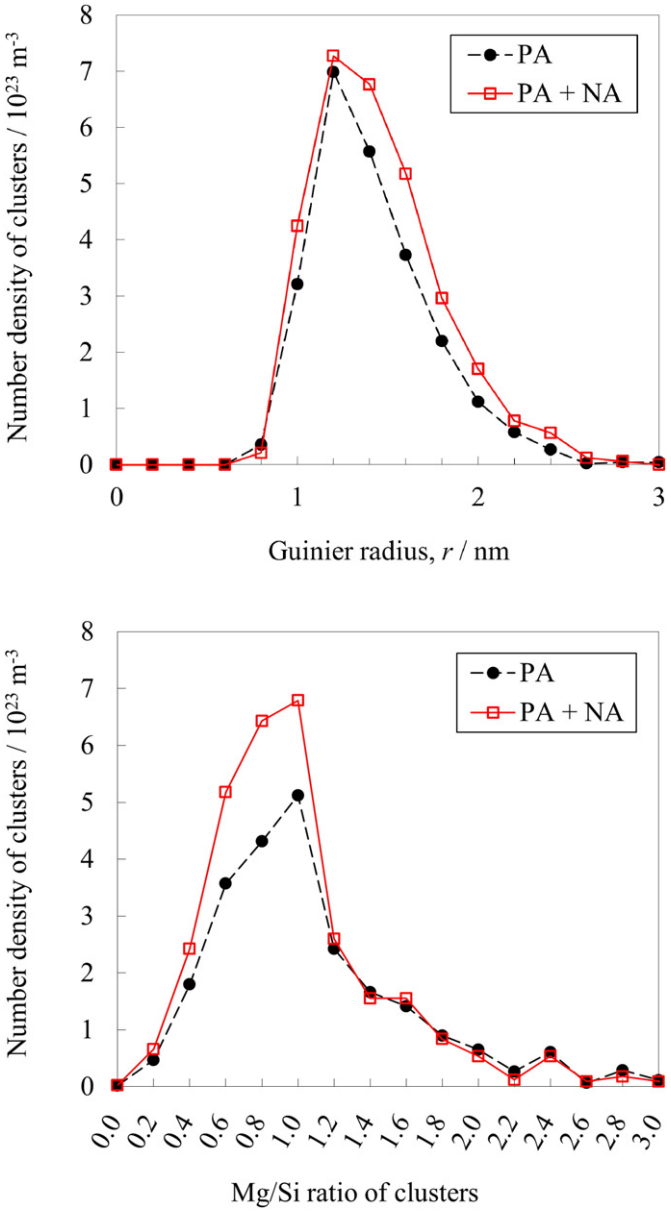

Fig. 3. (a) Size distribution of clusters in the materials after PA at 90 °C for 18 ks (PA) and subsequent NA for 4.0×10^4 ks (PA + NA). (b) Relationship between Mg/Si ratio and number density of clusters in the materials after PA at 90 °C for 18 ks (PA) and subsequent NA for 4.0×10^4 (PA + NA).

Kinetically, the formation and growth of clusters is determined by the vacancy-assisted diffusion of solute atoms to clusters or by the solute attachment at the cluster–matrix interface [25]. It is suggested the interaction energy between Si atoms and vacancies is lower than that between Mg atoms and vacancies in Al [26]. Even at equilibrium vacancy concentrations, the diffusivity of Si is expected to be greater than that of Mg. This difference increases as the temperature falls, being a factor of 3 at RT [15]. From the viewpoint of supersaturation of solute Mg and Si, clusters formed during PA have a higher average Mg/Si ratio as shown in Table 2. The APT analysis can measure the residual solute concentrations of Mg and Si after PA, which are 0.49 at.% and 0.84 at.%, respectively. The solute Mg/Si ratio after PA, 0.58, is quite lower than that of the initial value (0.78) based on the alloy composition. This decrease of Mg/Si ratio in matrix concentration should increase the attachment rate of the clusters and solute Si at the cluster–matrix interfaces during subsequent NA. Actually, Torsæter et al. showed that the average Mg/Si ratio of clusters is associated with the alloy composition [8]. From the abovementioned point, it is believed that the greater diffusivity of Si with respect to Mg in combination with the high Si concentration in the matrix can contribute to higher relative Si contents in clusters formed during prolonged RT storage after PA. In addition, from accurate lattice parameter measurements of alloys, it is estimated that Mg atoms are ~12% larger than Al atoms, whereas Si atoms are ~6% smaller [27]. The PA clusters which have a higher average Mg/Si ratio might favor preferential aggregation of Si atoms in order to reduce the strain energy caused by the difference in atomic sizes.

As for the BH response, the prolonged NA after PA inhibits the hardness increase during the BH treatment as shown in Fig. 2. It has been suggested that Si-rich clusters which are prone to be formed at the initial stage of NA after solution treatment do not directly transform into the β″ phase in terms of the thermal stability [28] and ion binding property for the bonding of Si–Si atoms [29]. It was proven that the typical Si-rich (Mg/Si ratio ≤ 0.4) clusters formed during NA can neither be dissolved nor grow further during artificial aging at 170 °C for up to 3.6 ks [14]. On the other hand, it was found that an increase of small clusters with various Mg/Si ratios does not promote the BH response, whereas large (typically larger than 2.0 nm in radius) clusters with a uniform Mg/Si ratio play an important role in hardening during the BH treatment [13]. The present work has revealed that a long-term NA after PA increases the number density of Si-rich clusters. Although the volume of the large clusters increases during the long-time NA, most of them have low Mg/Si ratio as shown in Fig. 3. Consequently, it is speculated that the deterioration of the BH response in the PA + NA material is mainly caused by the increase of the Si-rich clusters.

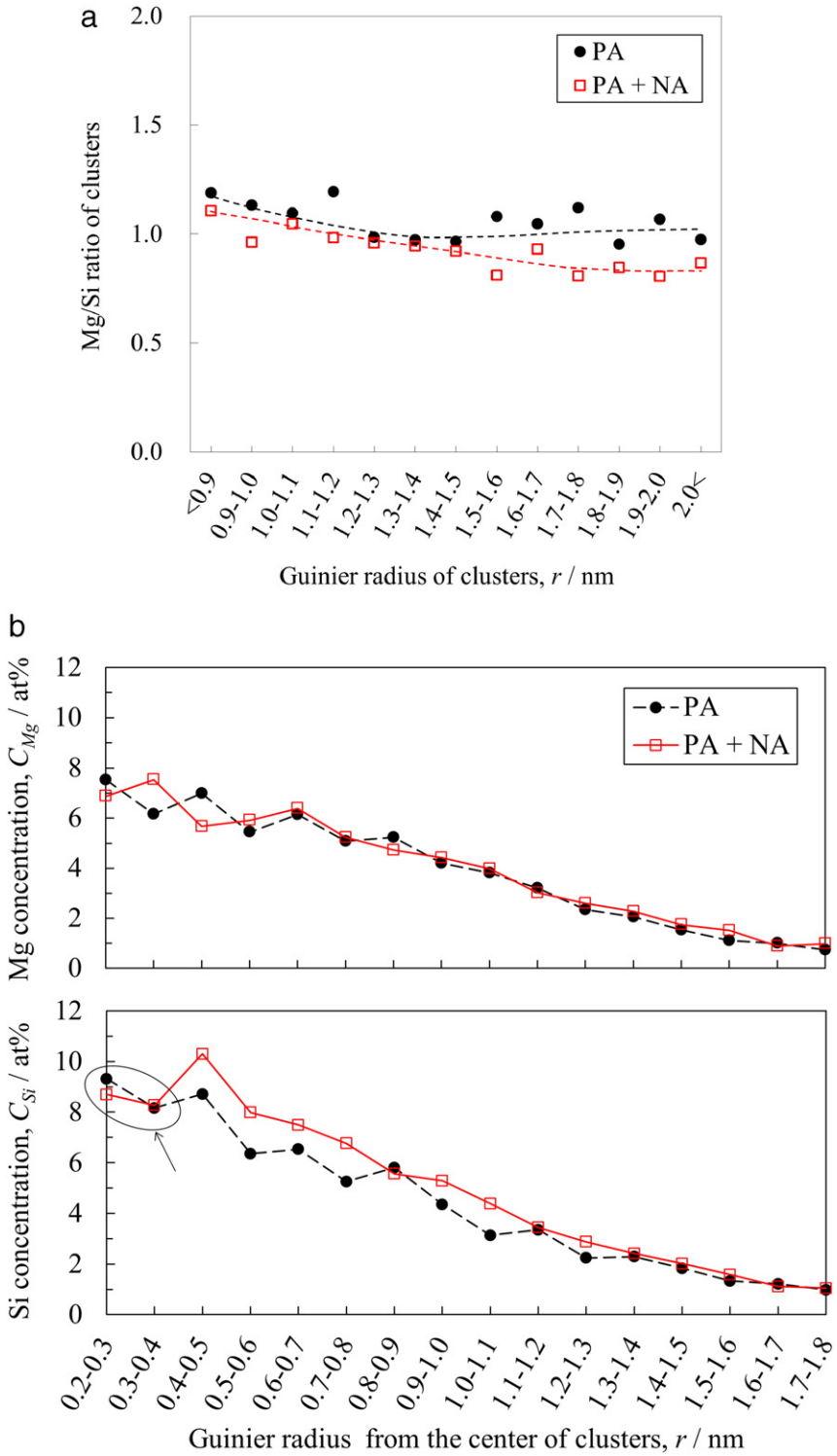

Fig. 4. (a) Mg/Si ratio of clusters plotted against cluster size ranges in the materials after PA at 90 °C for 18 ks (PA) and subsequent NA for 4.0×10^4 ks (PA + NA). (b) Average concentration profiles of Mg and Si with distance from the center of clusters with radius larger than 1.5 nm in the materials after PA at 90 °C for 18 ks (PA) and subsequent NA for 4.0×10^4 ks (PA + NA). There is little difference in Si concentration of below 0.4 nm in Guiner radius from the center of clusters between the PA and PA + NA materials as indicated by a circle and arrow, while in the ranges of larger radius the Si concentration in the PA + NA material is remarkably higher than in the PA material.

In summary, the present work showed that NA for 4.0×10^4 ks after PA at 90 °C for 18 ks inhibits the hardness increase during the BH treatment in an Al–0.62Mg–0.93Si (mass%) alloy. NA after PA leads to an increase in the number density, whereas a decrease in the average Mg/Si ratio of clusters, namely, Si-rich clusters mainly increase during the long-time storage at RT. The Si concentration of larger clusters in the PA + NA material is remarkably higher than in the PA material except for the region near the center of clusters. It is believed that a long-term NA after PA promotes the preferential aggregation of solute Si toward clusters formed during PA rather than the independent formation of Si-based clusters. It is speculated that the deterioration of the BH response by the prolonged NA after PA is mainly originated from the increase of the Si-rich clusters.

References

[1] D.J. Lloyd, in: D.S. Wilkinson, W.J. Poole (Eds.), Advances in Industrial Materials, Canadian Institute of Mining, Metallurgy, and Petroleum, Montreal, Canada 1998, pp. 3–17.
[2] S. Pogatscher, H. Antrekowitsch, H. Leitner, T. Ebner, P.J. Uggowitzer, Acta Mater. 59 (2011) 3352–3363.
[3] G.A. Edwards, K. Stiller, G.L. Dunlop, M.J. Couper, Acta Mater. 46 (1998) 3893–3904.
[4] J. Banhart, M.D.H. Lay, C.S.T. Chang, A.J. Hill, Phys. Rev. B 83 (2011) 014101.
[5] C.D. Marioara, S.J. Andersen, J. Jansen, H.W. Zandbergen, Acta Mater. 51 (2003) 789–796.
[6] M. Murayama, K. Hono, Acta Mater. 47 (1999) 1537–1548.
[7] A. Serizawa, S. Hirosawa, T. Sato, Metall. Mater. Trans. A 39 (2008) 243–251.
[8] M. Torsæter, H.S. Hasting, W. Lefebvre, C.D. Marioara, J.C. Walmsley, S.J. Andersen, R. Holmestad, J. Appl. Phys. 108 (2010) 073527.
[9] P.A. Rometsch, L.F. Cao, X.Y. Xiong, B.C. Muddle, Ultramicroscopy 111 (2011) 690–694.
[10] L. Cao, P.A. Rometsch, M.J. Couper, Mater. Sci. Eng. A 559 (2013) 257–261.
[11] L. Cao, P.A. Rometsch, M.J. Couper, Mater. Sci. Eng. A 571 (2013) 77–81.
[12] R.K.W. Marceau, A. de Vaucorbeil, G. Sha, S.P. Ringer, W.J. Poole, Acta Mater. 61 (2013) 7285–7303.
[13] Y. Aruga, M. Kozuka, Y. Takaki, T. Sato, Metall. Mater. Trans. A 45 (2014) 5906–5913.
[14] Y. Aruga, M. Kozuka, Y. Takaki, T. Sato, Mater. Sci. Eng. A 631 (2015) 86–96.
[15] M.W. Zandbergen, Q. Xu, A. Cerezo, G.D.W. Smith, Acta Mater. 101 (2015) 136–148.
[16] K. Yamada, T. Sato, A. Kamio, Mater. Sci. Forum 331–337 (2000) 669–674.
[17] L. Zhen, S.B. Kang, H.W. Kim, Mater. Sci. Technol. 13 (1997) 905–910.
[18] S. Esmaeili, X. Wang, D.J. Lloyd, W.J. Poole, Metall. Mater. Trans. A 34 (2003) 751–763.
[19] P.A. Rometsch, S.X. Gao, M.J. Couper, in: H. Weiland, A.D. Rollett, W.A. Cassada (Eds.),Proc. 13th International Conference on Aluminium Alloys (ICAA-13) 2012, pp. 15–20.
[20] Y. Takaki, T. Masuda, E. Kobayashi, T. Sato, Mater. Trans. 55 (2014) 1257–1265.
[21] M.K. Miller, Atom Probe Tomography, Kluwer Academic/Plenum Publishers, New York, 2000.
[22] J.M. Hyde, C.A. English, in: G.E. Lucas, L. Snead, M.A. Kirk, R.G. Elliman (Eds.), Materials Research Symposia, 650, Materials Research Society, Pittsburgh, PA 2001, p. R6.6.
[23] I. Dutta, S.M. Allen, J. Mater. Sci. Lett. 10 (1991) 323–326.
[24] A.K. Gupta, D.J. Lloyd, Metall. Mater. Trans. A 30 (1999) 879–883.
[25] J.W. Christian, The Theory of Transformations in Metals and Alloys: Part I Equilibrium and General Kinetic Theory, second ed. Pergamon Press Ltd., Oxford, 1975.
[26] T. Hoshino, F. Nakamura, J. Metastable Nanocryst. Mater. 24–25 (2005) 237–240.
[27] H.W. King, J. Mater. Sci. 1 (1966) 79–90.
[28] J.-H. Kim, E. Kobayashi, T. Sato, Mater. Trans. 56 (2015) 1771–1780.
[29] H. Adachi, H. Nakanishi, M. Asano, J. JILM 65 (2015) 411–415.